Critical structural fluctuations of proteins upon thermal unfolding challenge the Lindemann criterion

Marina Katava[a], Guillaume Stirnemann[a], Marco Zanatta[b], Simone Capaccioli[c], Maria Pachetti[c], K. L. Ngai[c], Fabio Sterpone[a,1], and Alessandro Paciaroni[d,1]

[a]Laboratoire de Biochimie Théorique, Institut de Biologie Physico-Chimique, CNRS Unité Propre de Recherche 9080, Université Paris Diderot, Sorbonne Paris Cité, 75005 Paris, France; [b]Dipartimento di Informatica, Università di Verona, 37134 Verona, Italy; [c]Dipartimento di Fisica, Università di Pisa and Istituto per i Processi Chimico-Fisici—Consiglio Nazionale delle Ricerche, 56127 Pisa, Italy; and [d]Dipartimento di Fisica e Geologia, Università di Perugia, 06123 Perugia, Italy

Edited by Martin Gruebele, University of Illinois at Urbana-Champaign, Urbana, IL, and approved July 19, 2017 (received for review May 3, 2017)

Internal subnanosecond timescale motions are key for the function of proteins, and are coupled to the surrounding solvent environment. These fast fluctuations guide protein conformational changes, yet their role for protein stability, and for unfolding, remains elusive. Here, in analogy with the Lindemann criterion for the melting of solids, we demonstrate a common scaling of structural fluctuations of lysozyme protein embedded in different environments as the thermal unfolding transition is approached. By combining elastic incoherent neutron scattering and advanced molecular simulations, we show that, although different solvents modify the protein melting temperature, a unique dynamical regime is attained in proximity of thermal unfolding in all solvents that we tested. This solvation shell-independent dynamical regime arises from an equivalent sampling of the energy landscape at the respective melting temperatures. Thus, we propose that a threshold for the conformational entropy provided by structural fluctuations of proteins exists, beyond which thermal unfolding is triggered.

neutron scattering | molecular dynamics simulation | protein dynamics | Lindemann criterion | cell thermal stability

Local subnanosecond timescale structural fluctuations are needed for proteins to function (1). A prototypical case is myoglobin, where correlated sidechain motions take place while carbon monoxide moves from its primary docking site into secondary pockets (2). Without fast structural dynamics, proteins could not even fold in their native structure. In fact, inherent rearrangements of protein backbone and sidechains allow, in the earliest phase of folding, for searching of small local metastable structures and eventually the lowest-energy native conformation in a local-to-global process (3, 4) as interpreted in terms of the conformational substate theory (5). Within this framework, subnanosecond timescale motions correspond to jumps among nearly equal minima in the multidimensional free energy landscape (EL) that defines the hierarchical dynamics of proteins. Such motions are extremely sensitive to the amount and the nature of solvent surrounding the protein surface (6–8). At room temperature, both the amplitude and the rate of these dynamics are dramatically reduced when proteins are embedded in sugar–glass matrices (1). In these conditions, proteins also show much larger melting temperatures, T_m, than in physiological aqueous media. This suggests that the external confinement restricts both local and global dynamical processes, eventually leading to unfolding (9). To some extent, such a picture is consistent with the hypothesis that the structural rigidity of thermophilic proteins grants their stability at extreme temperatures (10). Fast internal dynamics are also important in the modulation of the stability of proteins because they are a major component of the conformational entropy (11–13).

Since subnanosecond protein internal motions are strongly driven by the temperature, it is relevant to follow the changes of their amplitude along the pathway toward the thermal unfolding. Proposed several years ago, borrowing the Lindemann criterion for crystal melting (14), an oversimplified but insightful view is that thermal unfolding of proteins corresponds to the crossover from a solid-like to a liquid-like character of native proteins' core (15). Considerable experimental and theoretical efforts have been made to characterize the microscopic details of protein melting events (16–18), yet the atomic traits of the dynamic mechanisms leading to protein structural destabilization are still elusive.

Precise information on the fast structural dynamics in proteins can be effectively obtained by incoherent neutron scattering (NS). This experimental technique is highly sensitive to motions of hydrogen atoms that are in turn distributed almost homogeneously within the biomolecules and can be contrasted with respect to perdeuterated solvent (19). Elastic incoherent NS (EINS), which we exploited in this work, provides a quantitative measure of the amplitude of protein internal motions in the experimentally accessible timescale (from pico- to nanosecond) in terms of the hydrogen mean-square displacements (MSD). The MSD measured on approaching the protein melting temperature result from the average over all of the possible conformations acquired by the proteins, with contribution from folded and unfolded states. Molecular dynamics (MD) based on atomistic models is a unique tool to dissect these separate contributions, provided that the temperature-dependent conformational landscape is effectively sampled. To this purpose we deployed an enhanced sampling method to assess protein thermal response and melting in silico, i.e., replica exchange with solute tempering (REST2) (20, 21), and support the EINS results.

Significance

In 1910 F. A. Lindemann introduced a practical criterion to predict the melting of crystals on the basis of the relative magnitude of thermal atomic fluctuations and the crystal lattice constant. The idea of a critical threshold for the local motions that would trigger melting also in disordered media like proteins has inspired important subsequent investigations. Here, a common scaling toward a constant value for the local fluctuations of a model protein in different environments is proved when approaching the unfolding temperature. This landmark result not only sheds unique light on the relationship between protein flexibility and stability, but also opens the possibility to predict protein unfolding in special environments (e.g., the cell interior) by following thermal local fluctuations.

Author contributions: F.S. and A.P. designed research; M.K., G.S., M.Z., S.C., M.P., K.L.N., F.S., and A.P. performed research; M.K., G.S., F.S., and A.P. analyzed data; and F.S. and A.P. wrote the paper.

The authors declare no conflict of interest.

This article is a PNAS Direct Submission.

[1]To whom correspondence may be addressed. Email: alessandro.paciaroni@unipg.it or fabio.sterpone@ibpc.fr.

This article contains supporting information online at www.pnas.org/lookup/suppl/doi:10.1073/pnas.1707357114/-/DCSupplemental.

Here, we studied the amplitude of fast structural fluctuations for a model globular protein, chicken egg-white lysozyme (CEWL), in the presence of different solvent matrices, from water to glassy networks, to sample increasingly stable systems in a wide temperature range up to the melting. We show that, even if the fast internal dynamics of the biomolecule are largely tuned by its molecular environment, when the solvent-dependent melting temperature is approached, the protein MSD converge to a common value. This trend indicates that the solvation environment preserves proteins from melting by controlling the amplitude of their local fluctuations, until a certain critical value of conformational entropy is reached, at high enough temperature, and unfolding events become predominant.

Results

MSD of CEWL in Different Environments Up to Their Melting Temperatures. EINS experiments have been performed on CEWL in the presence of the different perdeuterated matrices D2O, glycerol, and glucose, at the backscattering spectrometer IN13 [Institut Laue-Langevin (ILL), Grenoble, France]. This instrument is suitable to explore protein motions faster than $\sim$150 ps. Differential scanning calorimetry (DSC) measurements have shown that the melting temperature of CEWL is strongly affected by the surrounding shell, passing from $T^{wat}_{m,exp} = 340$ K for CEWL hydrated with 0.4 g water per gram of dry protein (22) to $T^{gly}_{m,exp} = 370$ K and $T^{glu}_{m,exp} = 400$ K for CEWL embedded in 1:1 (gram protein per gram solvent) matrices of glycerol (9) and glucose (Fig. S1), respectively. In Fig. 1*A* we show the NS elastic intensity $I_{el}(Q, T)$ of the different samples as a function of the wavevector transfer Q at 300 K and at the melting temperatures. In the incoherent approximation, the decay of $I_{el}(Q, T)$ vs. Q comes from vibrational and diffusive reorientational motions of protein hydrogen atoms, occurring within the experimentally accessible timescale and thus not contributing to the elastic part of the signal. The trend of $I_{el}(Q, T)$ at room temperature is indicative of thermal fluctuations whose extent increases more and more when the protein is surrounded by progressively less viscous matrices, i.e., going from glucose to glycerol and from glycerol to water. Very interestingly, the elastic intensities of CEWL in the different matrices collapse into a single curve at their respective $T_{m,exp}$. This is clear model-independent evidence of very similar protein dynamics approaching the thermal unfolding in the different environments. The quantitative assessment of the amplitude of protein thermal fluctuations is reported in Fig. 1*B* in terms of MSD extracted from $I_{el}(Q, T)$ in a wide temperature range from 20 K up to the melting temperature (*Materials and Methods* and *Double-Well Model*). The derived MSD account for the heterogeneous dynamics of protein hydrogen atoms within the timescale defined by the energy resolution of the spectrometer (23). It is commonly accepted that above 100 K, various protein local relaxations give rise to anharmonic onsets (24). The most evident of these contributions is the protein dynamic transition (PDT), due to the so-called β relaxation of the solvation shell entering the experimentally accessible time window and triggering the reorientational dynamics of protein sidechains (24–26). The solvent-driven character of the PDT is clear, as we can qualitatively identify that it takes place at quite different temperatures in the investigated systems, namely at about 230 K, 280 K, and 360 K for, respectively, CEWL plus D_2O, glycerol, and glucose (Fig. 1*B*) (7, 24, 27). After this transition, the MSD increase with an environment-dependent rate, up to a certain environment-dependent melting point. However, as expected from the surprising behavior of $I_{el}(Q, T)$, the protein MSD approach a common value in proximity to its specific T_m.

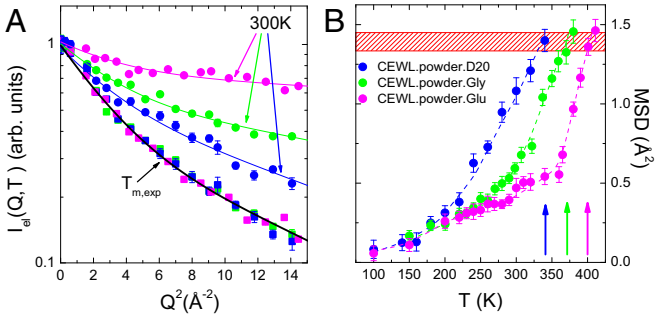

Fig. 1. Protein fast structural fluctuations from EINS. (*A*) Elastic intensity of CEWL+D_2O (blue), CEWL+glycerol (green), and CEWL+glucose (pink) at 300 K and at the respective melting temperatures. The curves are fits to the data with the double-well model. (*B*) MSD of CEWL and melting temperatures (arrows) in the presence of different environments (colors as in *A*). The red hatched area highlights the region of critical MSD, corresponding to the melting of CEWL in the different environments. Dashed lines are guides to the eye.

A Lindemann-Like Criterion for the Melting of Proteins. In the case of solids, the Lindemann criterion states that crystals liquefy when the amplitude of atomic thermal vibrations exceeds a fraction of the interatomic spacing, typically in the range around 0.15 (14). This venerable and old, but very useful, idea has been generalized to be applied to inhomogeneous systems (28) and proteins (15), where the Lindemann parameter Δ_L has been redefined as the ratio between the root of the mean-squared fluctuations (MSF) and the most-probable nonbonded near-neighbor distance a in the system; i.e., $\Delta_L = \sqrt{MSF}/a$. Here, in analogy with that generalization, we estimate the Lindemann parameter from the hydrogen MSD, by using the relationship $\Delta_L = \frac{1}{a}\sqrt{\frac{MSD}{2}}$, taking into account the fact that in the harmonic approximation $MSD = 2MSF$. In CEWL, the most-probable nonbonded near-neighbor distance, calculated from the simulated structures, is $a = 4.75$ Å. In Fig. 2 we show that the experimental Lindemann parameter Δ^{exp}_L approaches a common value of $\sim$0.17 at $T_{m,exp}$, regardless of whether the protein surface is surrounded by water or by glassy matrices.

This value results from the combined amplitudes of fluctuations from folded and unfolded states, with the contribution from the latter becoming predominant as the melting temperature is crossed. To dissect the separate contributions from native and unfolded states we exploit an in silico approach based on MD simulations.

Probing the Melting Temperature in Silico. To study the melting process for two of the investigated systems, i.e., CEWL in powder in the presence of water and glycerol solvents (Fig. S2), we performed enhanced sampling via the REST2 method. To distinguish the folded and the unfolded states, we used the root-mean-square distance (C_α-RMSD) computed for C_α backbone atoms as a reaction coordinate, benchmarking the temperature-dependent protein structure trajectories against an equilibrated structure at $T = 300$ K. As shown in Fig. 3*A*, C_α-RMSD is an appropriate choice, since it provides a measure of the biomolecule deformation in response to thermal excitation. Based on the distribution of the C_α-RMSD in the trajectories (Fig. 3*A*, *Inset*), we chose the threshold C_α-RMSD = 4.0 Å as the surface separating the folded and the unfolded states and determined the fraction of the folded state f as a function of temperature by applying a smoothing function to the C_α-RMSD values (Fig. 3*B*). From the stability curves we inferred the melting temperatures for the two systems, with $T^{wat}_{m,sim} = 444$ K and $T^{gly}_{m,sim} = 524$ K. As expected, the in silico melting

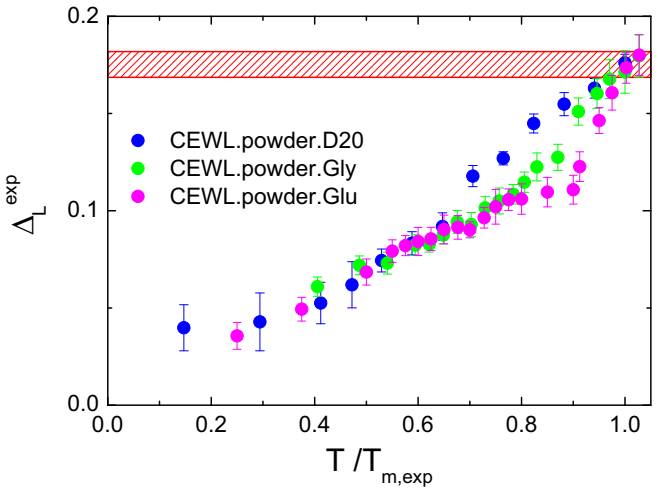

Fig. 2. Scaling law of protein fast fluctuations by EINS. Shown is the experimental Lindemann parameter for CEWL in the presence of different environments as a function of the reduced temperature $T/T_{m,exp}$. The red hatched area highlights the region of critical MSD, corresponding to the protein melting in the different environments.

temperatures are much higher than the experimental ones, due to two concomitant factors. First, besides convergence issues that are always difficult to assess, we should recall that atomistic force fields generally overestimate the melting temperature (30). In addition, and probably more important, in our enhanced sampling calculations only one protein in the system is thermally excited to explore folding/unfolding events, while the remaining proteins act as stable crowders. This is a necessary strategy to make the calculation feasible. Conversely, in the experimental samples all of the proteins are destabilized in proximity to melting, thus making the effective confinement felt by a single protein softer than in simulations. However, despite the intrinsic limits of the current numerical methods, the recovered $T_{m,sim}$ for CEWL embedded in glycerol is considerably higher than that of the hydrated protein, in qualitative agreement with DSC (9, 22).

On approaching the melting, the number of conformational states visited by the proteins suddenly increases, due to the activated mobility of specific unfolded fragments. In Fig. 3*C* the expansion of the visited conformational space is represented by the network of configurations clustered according to C_α-RMSD. At any temperature the number of backbone substates visited by the protein is smaller in glycerol than in water. This is probably due to the distinct steric hindrance and to the different number of hydrogen bonds the solvents can form with the protein. Both these effects influence directly or through the sidechains dynamics the backbone rearrangements. However, a common rescaling for the visited conformational substates, similar to the MSD trend, is recovered on approaching $T_{m,sim}$ when they are normalized with respect to the number of substates sampled at ambient conditions (Fig. S3).

According to secondary structure calculations, in both systems the unfolded state is mainly characterized by the systematic disruption of the native β-strand [Thr40-Gly54] and unwinding of helices [Trp108-Gly117] and [Asp119-Arg125] at the C terminus (Fig. S4). Although the fine molecular details of unfolding depend on the solvation and on the crowding condition, we find weak spots consistent with those revealed in wide-angle X-ray diffraction (31) and circular dichroism, FTIR, and NMR (32) experiments. The disruption of the β structure anticipates the complete melting of the protein, and in agreement with experimental data (32), at $T_{m,sim}$, the system has lost half of its helical content.

MD Simulations Provide Insight into Protein Fluctuations in Folded and Unfolded States. From REST2 simulations, representative unfolded configurations were extracted for the two systems and used to reconstruct the thermal scaling of the MSD for both folded and unfolded states; see Fig. 4*A* and Fig. S5 for details. The MSD for the unfolded state are slightly larger than for the folded state, and the difference increases with temperature. This is a signature of a comparable packing of the folded and the unfolded conformations under the strong confinement in the powder environment. In fact, in the present systems, the fraction of volume occupied by the biomolecules is $\phi \sim 65\%$, an extreme crowding condition even compared with the typical value of the intracellular space ($\phi \sim 30\%$) (33).

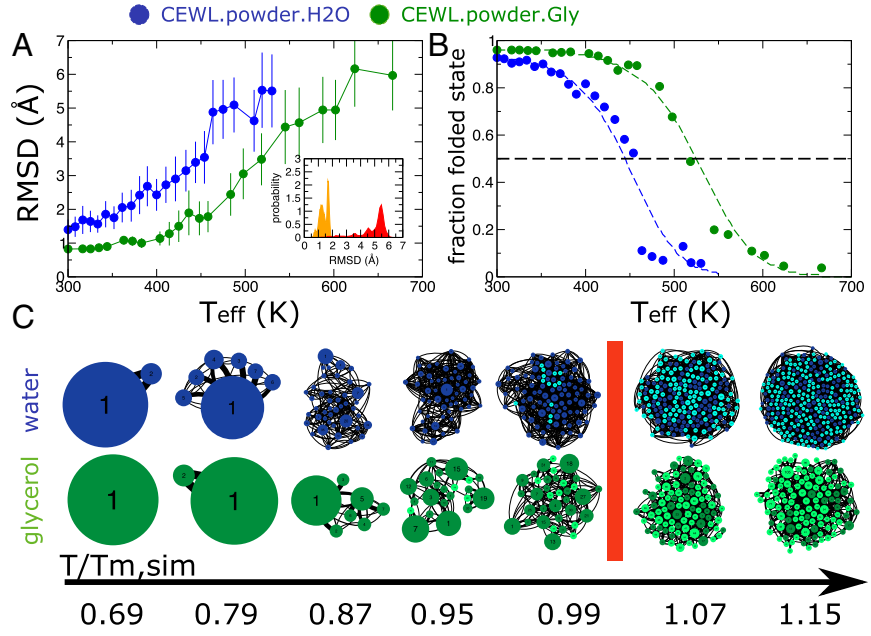

Fig. 3. Definition of folded and unfolded states in silico. (*A*) Average C_α-RMSD values obtained from REST2 simulations at different effective temperatures for CEWL+water (blue circles) and CEWL+glycerol (green circles). *Inset* shows probability distribution of the C_α-RMSD values at room (orange) and high (red) temperatures. (*B*) Stability curves of CEWL in silico. Data shown in circles are derived from RMSD distributions and the two-state model, while the dashed lines represent fits to the data (29). (*C*) The conformational states sampled by the CEWL protein are represented as networks of states with the size of the nodes proportional to the state occupancy and with darker colors for the native-like conformations and lighter colors for unfolded-like conformations. The data correspond to selected temperatures and are represented in the $T/T_{m,sim}$ scale.

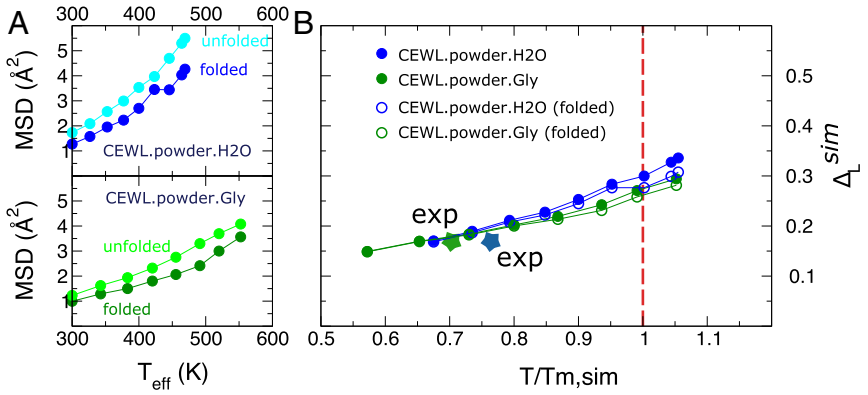

Fig. 4. Scaling law of protein fast fluctuations by simulations. (*A*) MSD from MD trajectories started from folded and unfolded configurations of CEWL in the presence of water and glycerol. The data for the unfolded state are obtained as the average over four independent runs initiated from different configurations of the unfolded CEWL extracted from the REST2 enhanced sampling. (*B*) Lindemann parameter obtained by combining the folded and unfolded states MSD, $MSD = f \cdot MSD_f + (1-f)MSD_u$, with f the fraction of folded states. In the same graph we report the folded-state contributions. The colored stars indicate the experimental points for the two systems.

From the numerical amplitude of protein structural fluctuations we provide an estimate of the protein conformational entropy difference between the folded and unfolded states, arising from the protein dynamics in the 150-ps timescale. We apply a simplified model where the protein sidechains behave as identical noninteracting classical moving particles (34). The entropy difference per residue between the unfolded and the folded states is estimated from the simulated MSD to be $\Delta S^{u/f} = \frac{3}{2} k_b \ln(MSD_u/MSD_f)$. At ambient conditions $\Delta S^{u/f} = 3.5$ J·(mol K)$^{-1}$ and 2.5 J·(mol K)$^{-1}$, for CEWL in the presence of water and glycerol, respectively. Similar values are determined at the melting temperatures. A tentative experimental assessment of $\Delta S^{u/f}$ for powder-like systems can be done by exploiting data reported by Weik and coworkers, where the MSD of the τ intrinsically disordered protein are compared with those of well-known globular proteins (35). Considering the intrinsically disordered protein as a model system for the unfolded state, at 300 K the ratio between the MSD of the τ protein and those of globular proteins gives a common per residue value of $\Delta S^{u/f} \simeq 4.7$ J·(mol K)$^{-1}$, in good agreement with our estimates. This estimated entropy change is three to four times smaller than the value of $\Delta S^{u/f} = 10.85$ J·(mol K)$^{-1}$ found in aqueous solution for α-amylase protein using the same model (34). Again, this gap is not surprising considering that crowding conditions in powders restrict the conformational space accessible to disordered chains, thus biasing unfolded conformations toward more compact states. For the sake of comparison, from MD simulations of folded and unfolded CEWL in aqueous solution we obtain $\Delta S^{f/u} \simeq 9$ J·(mol K)$^{-1}$ in much better agreement with the experimental value. All these data confirm that the performed sampling of the unfolded states in the powder condition is reasonable and that the decomposition of the experimental MSD via a two-state model is well grounded.

The Lindemann Criterion in Silico. According to the two-state model, the ensemble combination of the MSD allows us to derive the in silico Lindemann parameter Δ_L^{sim}, to be compared with the one measured by EINS. As shown in Fig. 4*B*, Δ_L^{sim} converges at melting for both systems to about 0.28. This value is larger than Δ_L^{exp}, owing to the shift of the in silico melting point with respect to the experimental one. This situation, due to a more rigid confinement performed by the unperturbed surrounding proteins in the simulations, mimics what is observed in solid superheating (36), where by suppressing surface melting by external coating, the crystal can be heated to much higher temperatures. At the new higher melting point the Lindemann parameter for bulk atoms is about 80% in excess of the equilibrium melting point, i.e., 0.22. vs 0.12, and approaches the value reported for the superficial atoms in standard surface-driven melting.

If we assume that the thermal scaling of the MSD is well reproduced by the molecular force field for a given protein conformational state, we can determine the Lindemann parameter from simulation data also at temperatures lower than $T_{m,sim}$, namely at the experimental melting. At $T_{m,exp}$ we find a value of $\Delta_L^{sim} \simeq 0.17 - 0.19$ for CEWL in the presence of water and glycerol, in excellent agreement with the EINS experimental assessments (star symbols in Fig. 4*B*) and previous estimates from simulations (15).

Fig. 4*B* shows that the Lindemann parameter calculated for the folded state alone is only slightly lower than the one resulting from the combination of folded and unfolded states. This is because the difference among the MSD in folded and unfolded conformations is small.

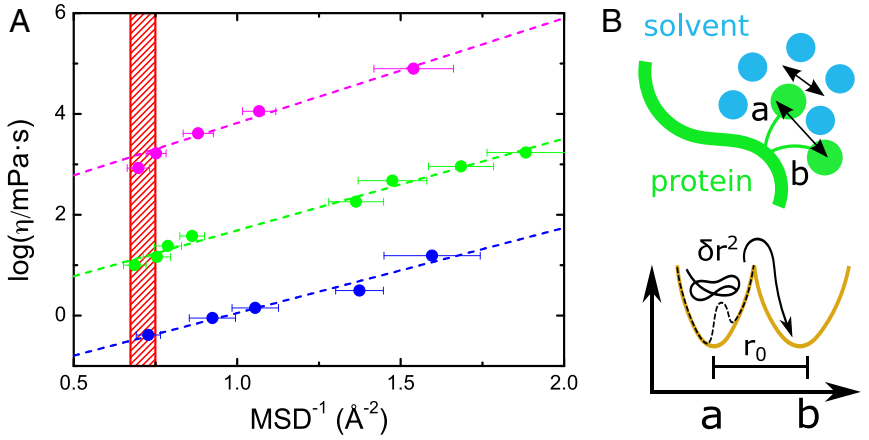

Fig. 5. HW model applied to protein dynamics close to melting. (*A*) Logarithm of bulk viscosity of the environments surrounding CEWL vs. reciprocal of MSD for CEWL in the different environments: CEWL+D_2O (blue), CEWL+glycerol (green), and CEWL+glucose (pink). Values of viscosities for water and glycerol have been taken from ref. 41, while the data for glucose come from ref. 42. The red hatched area highlights the region of critical MSD, corresponding to the melting of CEWL in the different environments. (*B*) Schematic representation of protein sidechains caged by the solvation shell. The average local rattling of hydrogen atoms in a conformational substate is sampled by NS and quantified by MSD. The magnitude of the displacement from a localized substate *a* toward a substate *b* can be accessed by fitting the HW model (38), relating MSD and the solvent viscosity η.

Discussion and Conclusions

We inquired into the amplitude of fast structural fluctuations in the high-temperature region up to the protein unfolding for the model protein CEWL, in different molecular environments. We found that, while the unfolding temperature changes significantly on changing the molecular solvation shell, a common value for the protein MSD is attained at the melting temperature. This determines for all systems an experimental Lindemann parameter $\Delta_L^{exp} \simeq 0.17$ close to the value found for superficial melting in crystals (36).

In its original definition, the Lindemann criterion is based solely on the behavior of the lattice constant and the atomistic fluctuations of the crystal phase (14). When transposed to the case of proteins, this criterion would correspond to the prediction of the biomolecule unfolding starting from the knowledge of thermal fluctuations in the folded state only. However, the common rescaling we experimentally found results from mixed contributions from the MSD in both folded and unfolded states. At T_m, where these states are equally populated, the relationship between the structural fluctuation amplitudes of proteins in the presence of different solvation shells can be summarized as follows: $\{MSD_f + MSD_u\}_{wat} = \{MSD_f + MSD_u\}_{gly} = \{MSD_f + MSD_u\}_{glu}$. To single out the contributions from the folded and unfolded states, we exploited MD simulations. Notably, for both the water and glycerol environments, the MSD of the folded and unfolded states are close in value and scale similarly with temperature (Fig. 4).

The roughness of the protein EL plays a key role in controlling protein fast fluctuations. Our results supports a picture where, close to the protein melting, the average landscapes of the combined free energy surfaces of the folded and unfolded states in the presence of different environments are very similar. In terms of simplified models of the local EL, this suggests that, at the respective T_ms, protein fast motions arise from an effective quadratic potential with very similar curvature. On the other hand, the trend of the protein dynamics on approaching the thermal unfolding also depends on the environment local viscosity, a quantity that cannot be accessed by experiments. Here we approximate the local viscosity at the protein–solvent interface with the bulk value of the solvent viscosity at the same thermodynamic conditions (37) in the temperature range between the PDT and T_m. In Fig. 5 we show that there is a linear relationship between the logarithm of the bulk viscosity of the environment surrounding the CEWL surface and the reciprocal of the protein MSD. The slopes of the curves for the different environments are very similar, thus indicating a common dependence of protein MSD on the viscous flow rearrangements of the surrounding shells. This behavior is reminiscent of the Hall–Wolynes (HW) model for glassy systems, relating viscosity and particle local fluctuations (38).

The HW model describes the molecular diffusion in a liquid as a series of local jumps between distinct minima in the EL (38–40). The macroscopic viscosity thus depends on the magnitude of these elementary displacements and the fluctuations in the local minima: $\eta = \eta_0 \cdot \exp[r_0^2/(2 < \delta r^2 >)]$, where η_0 is a reference viscosity (e.g., at the glass transition), r_0 is the displacement to overcome the barrier, and $< \delta r^2 >$ is the fluctuation in the localized state that matches the MSD at the timescale sampled in the EINS experiment (scheme in Fig. 5). In the present case, the observed correlation allows us to link the local protein conformational jumps to the bulk viscosity of the environment. In the HW model, the height of the barrier between protein conformational substates is proportional to r_0, and thus the similar slopes we obtain for the different environments indicate that, on approaching the respective melting, both the magnitude of local displacements and the rate-limiting barriers are similar in the studied systems. The average distance covered along the elementary jumps in the high-temperature range is $r_0 = 2.9 \pm 0.3$ Å. This value, which is twice as large as the protein MSD at the melting, is likely related to the large-amplitude sidechain torsional fluctuations. By exploiting the MSD_u and the MSD_f estimated from the REST2 simulations, we could show that the fast dynamics provide a significant contribution to the conformational entropy, thus affecting the protein thermal stability. The fact that, at the melting, this protein subnanosecond dynamical regime is environment independent strongly suggests that a certain critical value of the structural fluctuation amplitude is needed for triggering protein thermal unfolding.

One may wonder whether this behavior can be generalized to proteins other than CEWL. Actually, in Fig. S6 we show that the same value of the Lindemann parameter holds for hydrated myoglobin that we measured in an extended temperature range up to the melting, and it is reasonable also for other model proteins when the trend of the MSD is extrapolated in the range $T/T_m \gtrsim 0.8$. Particularly, it seems that Δ_L^{exp} does not depend significantly on the protein size, as crambin and BSA proteins, with quite different masses of about 5 kDa vs. 66 kDa, respectively, show the same trend. The similar behavior of hemoglobin suggests that Δ_L^{exp} is also independent of the presence of a quaternary structure. However, investigations still need to be made to verify this common behavior for other case studies, such as proteins from moderately thermophilic to hyperthermophilic organisms and their mesophilic homologs.

Additionally, the proposed Lindemann criterion for proteins could be used to predict the thermal stability of cells under the hypothesis that the cell's death temperature corresponds to the denaturation catastrophe of its proteome (43). This intriguing scenario is supported by the trend of the MSD from the proteome of psychrophile, mesophile, thermophile, and hyperthermophile bacteria, measured by EINS experiments similar to the ones of the present work (44). In Fig. S7 we show that, if we set the critical threshold to the MSD value we found for the unfolding of CEWL, i.e., $1.4\,\text{Å}^2$, then the amplitude of the thermal fluctuations of the bacterial proteome extrapolates to temperatures that quantitatively match the relevant temperatures where the organisms can no longer sustain growth, i.e., the maximum growth temperature. The similar macromolecular flexibility of organisms with largely different thermal stability at both their respective optimum growth (44) and maximum growth temperature marks a clear correlation of the protein stability/function trade-off at the cellular level. In this context, the universal scaling of the fast protein fluctuations at the melting is tantamount to a corresponding state principle, similar to what is conceptually used to explain the universal scaling of local hydrogen/deuterium exchange dynamics at proteins' functional temperatures (45).

In conclusion, the joined EINS and MD efforts allowed us to disclose the molecular mechanism underlying the thermal scaling of atomistic fluctuations at the unfolding temperature and provided a renewed picture of the Lindemann criterion for melting when applied to the soft disordered medium of proteins. The common value of MSD at the melting defines the critical value of the protein conformational entropy before the unfolded state becomes predominant. This principle might have practical applications in biotechnological and biomedical fields, since the knowledge of the thermal scaling of the protein atomistic fluctuations above the PDT would allow one to predict the melting temperatures in different environments, for instance in cell-like conditions. For this purpose forefront NS experiments could be designed to assess the stability of labeled cellular components by measuring their fast dynamics in a small temperature window.

Materials and Methods

Preparation of Samples and NS Experiments. Dialyzed salt-free CEWL and deuterated solvents were purchased from Sigma-Aldrich. The EINS measurements were performed on the backscattering spectrometer IN13 (ILL).

The elastic intensity (energy resolution with a half-width at half-maximum of $\Gamma = 4.5$ μeV) has been described in terms of the double-well model (25). For other details see *Preparation of Samples for Neutron Scattering Experiments*.

MD Simulations. MD simulations were performed on two lysozyme powder systems, one solvated in water and one in glycerol. The system setups match exactly the experimental samples described above. The simulations were performed with the CHARMM22/CMAP force field for proteins (46), CHARMM36 for the glycerol (47), and TIP3-CHARMM for water. We exploited the REST2 method (20, 21) to enhance the sampling of unfolding. For additional details see *In Silico System Preparation, REST2*, and *MD Simulations*.

ACKNOWLEDGMENTS. F.S. acknowledges funding from the European Research Council (FP7/2007–2013) Grant 258748, from the "Initiative d'Excellence" program from the French State (Grant "DYNAMO," ANR-11-LABX-0011-01), and high-performance computing resources from Grand Equipement National de Calcul Intensif (x2016076818). We thank the ILL for the allocation of beamtime.

1. Fenimore PW, Frauenfelder H, Mcmahon BH, Young RD (2004) Bulk-solvent and hydration-shell fluctuations, similar to α- and β-fluctuations in glasses, control protein motions and functions. *Proc Natl Acad Sci USA* 101:14408–14413.
2. Schotte F, Soman J, Olson JS, Wulff M, Anfinrud PA (2004) Picosecond time-resolved x-ray crystallography: Probing protein function in real time. *J Struct Biol* 147: 235–246.
3. Dill KA, MacCallum JL (2012) The protein-folding problem, 50 years on. *Science* 338:1042–1046.
4. Karplus M, Weaver DL (1976) Protein-folding dynamics. *Nature* 260:404–406.
5. Frauenfelder H, Petsko GA, Tsernoglou D (1979) Temperature-dependent X-ray diffraction as a probe of protein structural dynamics. *Nature* 280:558–563.
6. Zaccai G (2000) How soft is a protein? A protein dynamics force constant measured by neutron scattering. *Science* 288:1604–1607.
7. Paciaroni A, Cinelli S, Onori G (2002) Effect of the environment on the protein dynamical transition: A neutron scattering study. *Biophys J* 83:1157–1164.
8. Schiró G, et al. (2015) Translational diffusion of hydration water correlates with functional motions in folded and intrinsically disordered proteins. *Nat Commun* 6:6490.
9. Bell LN, Hageman MJ, Muraoka LM (1995) Thermally induced denaturation of lyophilized bovine somatotropin and lysozyme as impacted by moisture and excipients. *J Pharm Sci* 84:707–712.
10. Sterpone F, Melchionna S (2012) Thermophilic proteins: Insight and perspective from in silico experiments. *Chem Soc Rev* 41:1665–1676.
11. Lee AL, Wand J (2003) Microscopic origins of entropy, heat capacity and the glass transition in proteins. *Nature* 424:501–504.
12. Jarymowycz VA, Stone MJ (2006) Fast time scale dynamics of protein backbones: NMR relaxation methods, applications, and functional consequences. *Chem Rev* 106:1624–1671.
13. Doig AJ, Sternberg MJ (1995) Side-chain conformational entropy in protein folding. *Prot Sci* 4:2247–2251.
14. Lindemann FA (1910) The calculation of molecular vibration frequencies. *Physik Z* 11:609–612.
15. Zhou Y, Vitkup D, Karplus M (1999) Native proteins are surface-molten solids: Application of the Lindemann criterion for the solid versus liquid state. *J Mol Biol* 285:1371–1375.
16. Dobson CM (2003) Protein folding and misfolding. *Nature* 426:884–890.
17. Daggett V (2006) Protein folding-simulation. *Chem Rev* 106:1898–1916.
18. Lindorff-larsen K, Trbovic N, Maragakis P, Piana S, Shaw DE (2012) Structure and dynamics of an unfolded protein examined by molecular dynamics simulation. *J Am Chem Soc* 134:3787–3791.
19. Lovesey S (1988) *Theory of Neutron Scattering from Condensed Matter* (Oxford Univ Press, Oxford).
20. Wang L, Friesner R, Berne B (2011) Replica exchange with solute scaling: A more efficient version of replica exchange with solute tempering (rest2). *J Phys Chem B* 115:9431–9438.
21. Stirnemann G, Sterpone F (2015) Recovering protein thermal stability using all-atom Hamiltonian replica-exchange simulations in explicit solvent. *J Chem Theory Comput* 11:5573–5577.
22. Fujita Y, Noda Y (1978) Effect of hydration on the thermal denaturation of lysozyme as measured by differential scanning calorimetry. *Bull Chem Soc Jpn* 51:1567–1568.
23. Vural D, Hong L, Smith JC, Glyde HR (2015) Motional displacements in proteins: The origin of wave-vector-dependent values. *Phys Rev E Stat Nonlin Soft Matter Phys* 91:052705.
24. Capaccioli S, Ngai K, Ancherbak S, Paciaroni A (2012) Evidence of coexistence of change of caged dynamics at T(g) and the dynamic transition at T(d) in solvated proteins. *J Phys Chem B* 116:1745–1757.
25. Doster W, Cusack S, Petry W (1989) Dynamical transition of myoglobin revealed by inelastic neutron scattering. *Nature* 337:754–757.
26. Engler N, Ostermann A, Niimura N, Parak FG (2003) Hydrogen atoms in proteins: Positions and dynamics. *Proc Natl Acad Sci USA* 100:10243–10248.
27. Roh JH, et al. (2005) Onsets of anharmonicity in protein dynamics. *Phys Rev Lett* 95:038101.
28. Stillinger FH (1995) A topographic view of supercooled liquids and glass formation. *Science* 267:1935–1939.
29. Hawley SA (1971) Reversible pressure-temperature denaturation of chymotrypsinogen. *Biochemistry* 10:2436–2442.
30. Lindorff-Larsen K, Piana S, Dror R, Shaw D (2011) How fast-folding proteins fold. *Science* 334:517–520.
31. Hirai M, et al. (2004) Hierarchical map of protein unfolding and refolding at thermal equilibrium revealed by wide-angle x-ray scattering. *Biochemistry* 43:9036–9049.
32. Meersman F, et al. (2010) Consistent picture of the reversible thermal unfolding of hen egg-white lysozyme from experiment and molecular dynamics. *Biophys J* 99:2255–2263.
33. Wang Y, Sarkar M, Smith AE, Krois AS, Pielak GJ (2012) Macromolecular crowding and protein stability. *J Am Chem Soc* 134:16614–16618.
34. Fitter J (2003) A measure of conformational entropy change during thermal protein unfolding using neutron spectroscopy. *Biophys J* 84:3924–3930.
35. Gallat FX, et al. (2012) Dynamical coupling of intrinsically disordered proteins and their hydration water: Comparison with folded soluble and membrane proteins. *Biophys J* 103:129–136.
36. Jin Z, Gumbsch P, Lu K, Ma E (2001) Melting mechanisms at the limit of superheating. *Phys Rev Lett* 87:0557031–0557034.
37. Hynes J, Kapral R, Weinberg M (1979) Molecular theory of translational diffusion: Microscopic generalization of the normal velocity boundary condition. *J Chem Phys* 70:1456–1466.
38. Hall RW, Wolynes PG (1987) The aperiodic crystal picture and free energy barriers in glasses. *J Chem Phys* 86:2943–2948.
39. Xia X, Wolynes PG (2000) Fragilities of liquids predicted from the random first order transition theory of glasses. *Proc Natl Acad Sci USA* 97:2990–2994.
40. Cornicchi E, Onori G, Paciaroni A (2005) Picosecond-time-scale fluctuations of proteins in glassy matrices: The role of viscosity. *Phys Rev Lett* 95:158104.
41. Trejo González JA, Longinotti MP, Corti HR (2011) The viscosity of glycerol-water mixtures including the supercooled region. *J Chem Eng Data* 56:1397–1406.
42. Parks G, Barton L, Spaght ME, Richardson JW (1934) The viscosity of undercooled liquid glucose. *J App Phys* 5:193–199.
43. Dill KA, Ghosh K, Schmit JD (2011) Physical limits of cells and proteomes. *Proc Natl Acad Sci USA* 108:17876–17882.
44. Tehei M, et al. (2004) Adaptation to extreme environments: Macromolecular dynamics in bacteria compared in vivo by neutron scattering. *EMBO Rep* 5:66–70.
45. Závodszky P, Kardos J, Svingor A, Petsko GA (1998) Adjustment of conformational flexibility is a key event in the thermal adaptation of proteins. *Proc Natl Acad Sci USA* 95:7406–7411.
46. MacKerell AD, Feig M, Brooks CL 3rd (2004) Extending the treatment of backbone energetics in protein force fields: Limitations of gas-phase quantum mechanics in reproducing protein conformational distributions in molecular dynamics simulations. *J Comput Chem* 25:1400–1415.
47. Hatcher ER, Guvench O, MacKerell AD (2009) Charmm additive all-atom force field for acyclic polyalcohols, acyclic carbohydrates, and inositol. *J Chem Theory Comput* 5:1315–1327.
48. Phillips JC, et al. (2005) Scalable molecular dynamics with NAMD. *J Comput Chem* 26:1781–1802.
49. Schiro G, Natali F, Cupane A (2012) Physical origin of anharmonic dynamics in proteins: New insights from resolution-dependent neutron scattering on homomeric polypeptides. *Phys Rev Lett* 109:128102.
50. Wanderlingh UN, Corsaro C, Hayward RL, Bee M, Middendorf HD (2003) Proton mobilities in crambin and glutathione S-transferase. *Chem Phys* 292:445–450.
51. Stadler A, et al. (2006) *Temperature Dependence of Hemoglobin Dynamics in Intact Erythocytes* (Institut Laue-Langevin, Grenoble, France), Annual Rep IN13.
52. Stadler AM, Pellegrini E, Johnson M, Fitter J, Zaccai G (2012) Dynamics-stability relationships in apo- and holomyoglobin: A combined neutron scattering and molecular dynamics simulations study. *Biophys J* 102:351–359.
53. Hedoux A, et al. (2009) Thermostabilization mechanism of bovine serum albumin by trehalose. *J Phys Chem B* 113:6119–6126.
54. De Marco A, Lecompte JT, Llinás M (1980) Solvent and temperature effects on crambin, a hydrophobic protein, as investigated by proton magnetic resonance. *Eur J Biochem* 119:483–490.
55. Jansson H, Swenson J (2008) Dynamical changes of hemoglobin and its surrounding water during thermal denaturation as studied by quasielastic neutron scattering and temperature modulated differential scanning calorimetry. *J Chem Phys* 128:245104.
56. Tsuji A, Kaneko Y, Takahashi K, Ogawa M, Goto S (1982) The effects of temperature and pH on the growth of eight enteric and nine glucose non-fermenting species of gram-negative rods. *Microbiol Immunol* 26:15–24.
57. Huber R, et al. (1992) Aquifex pyrophilus gen. nov. sp. nov., represents a novel group of marine hyperthermophilic hydrogen-oxidizing bacteria. *Syst Appl Microbiol* 15:340–351.